Supplementary Material	Title
Supplementary Figure 1	Cross-polarization microscopy.
Supplementary Figure 2	Schematic of experimental protocol.
Supplementary Figure 3	Cell axes histograms.
Supplementary Figure 4	Crystal packing.
Supplementary Figure 5	Composite omit electron density maps.
Supplementary Figure 6	Electron density maps with hemes omitted.
Supplementary Figure 7	PEG-based LSP microjet images.
Supplementary Figure 8	Diffraction image from a mosaic crystal.
Supplementary Figure 9	NZ-test and L-test plots.
Supplementary Figure 10	Electron density maps against control data.
Supplementary Table 1	LCP and LSP crystal structures.
Supplementary Table 2	X-ray data and refinement statistics.
Supplementary Table 3	X-ray data statistics by resolution shell.
Supplementary Table 4	Refinement statistics by resolution shell.
Supplementary Note	
Supplementary References	

Supplementary Figure 1: Cross polarization microscopy.

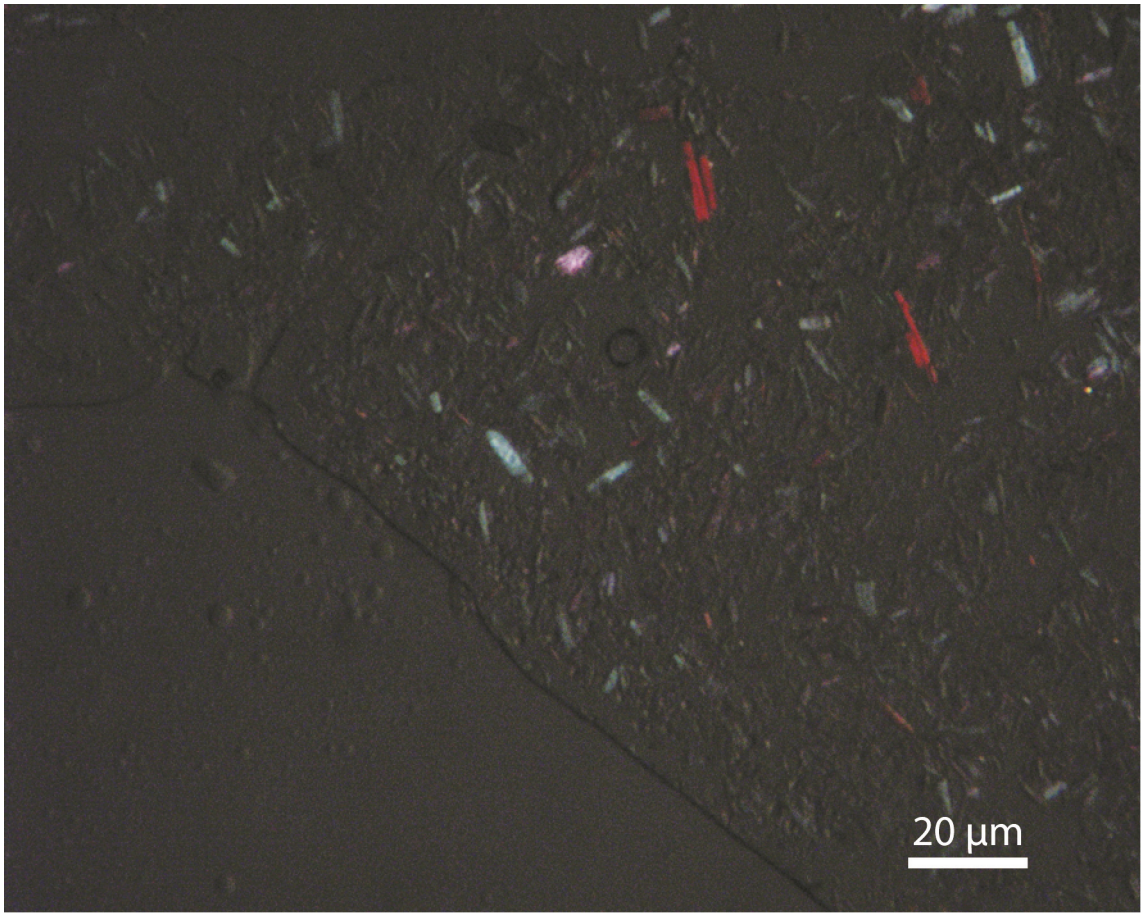

Cross polarization optical microscopy image of the crystallization setup shown in **Figure 1b**, indicating that the RC_{vir} microcrystals are birefringent. Longer crystals are approximately 20 µm long.

Supplementary Figure 2: Schematic of experimental protocol.

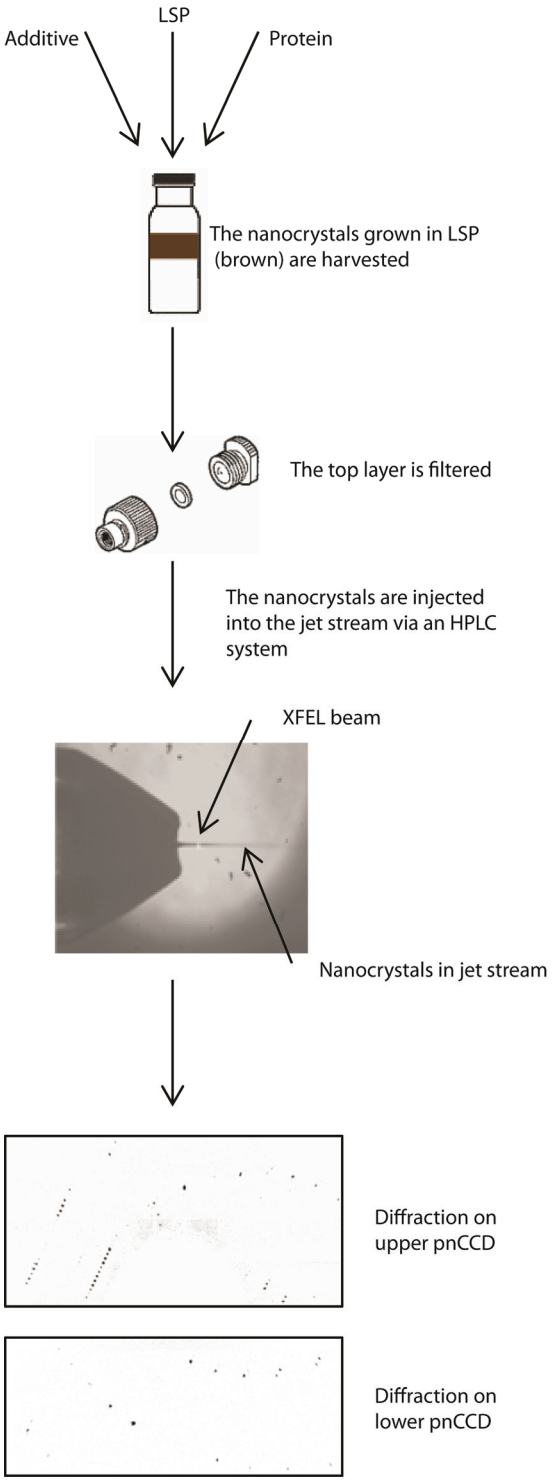

Schematic overview of the crystal growth, filtration, microjet injection and X-ray diffraction.

Supplementary Figure 3: Cell axes histograms.

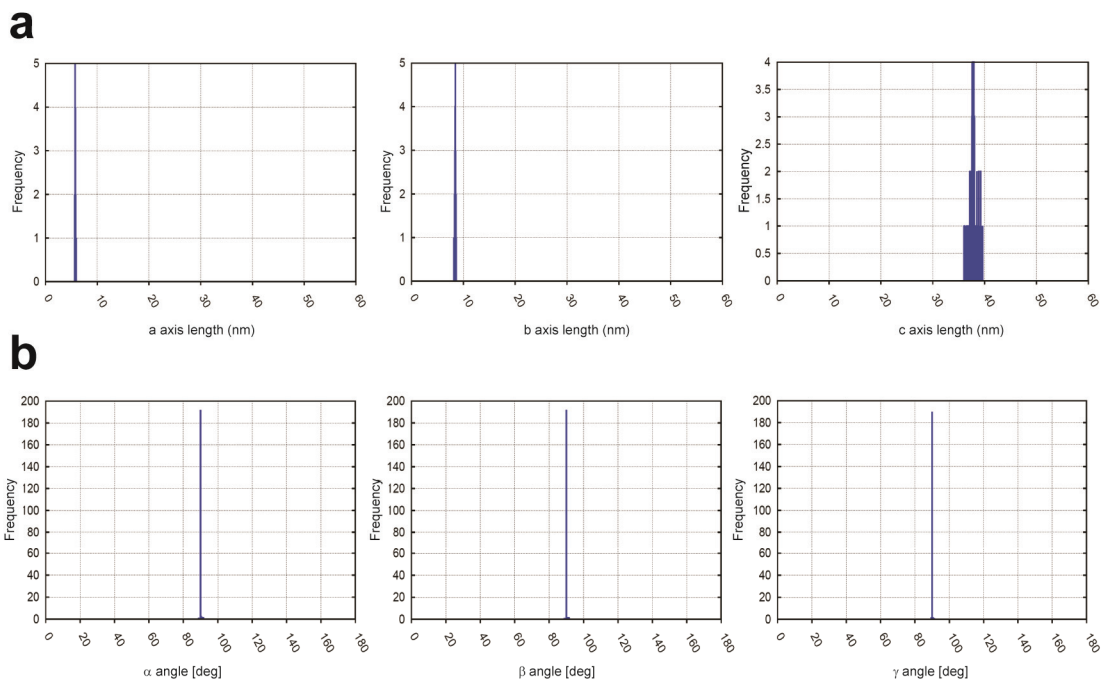

Histogram of (**a**) unit cell axes and (**b**) unit cell angles recovered from the 265 processed diffraction images.

Supplementary Figure 4: Crystal packing.

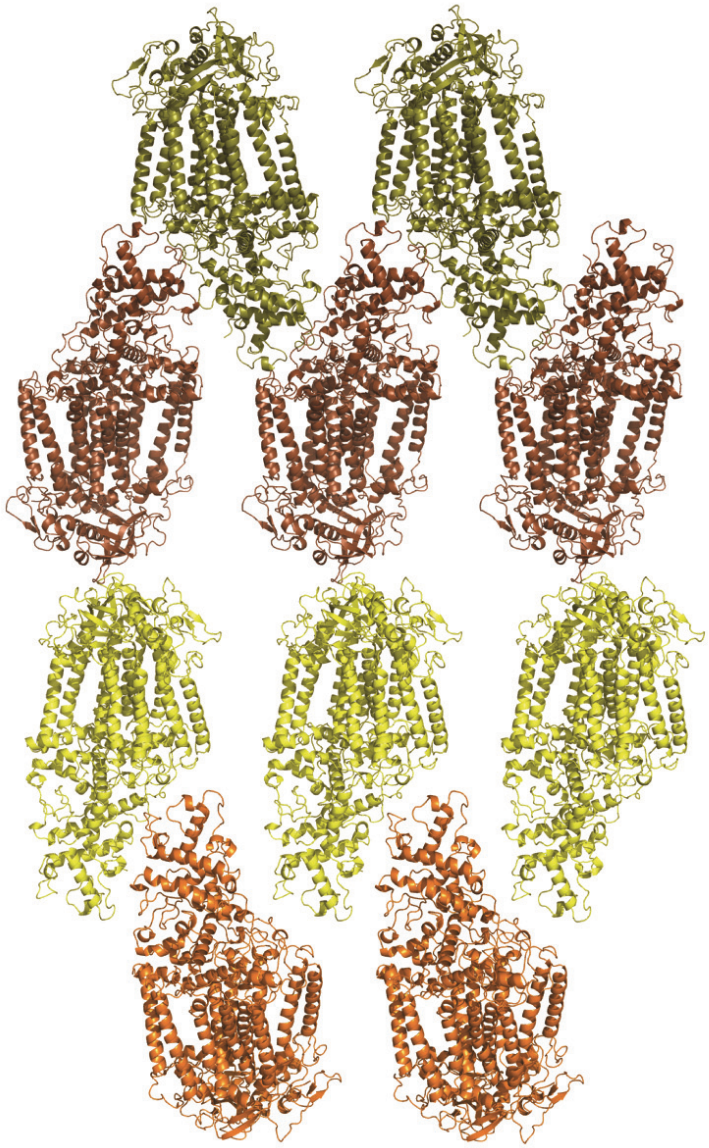

Crystal packing determined by molecular replacement for the LSP RC_{vir} microcrystals.

Supplementary Figure 5: Composite omit electron density maps.

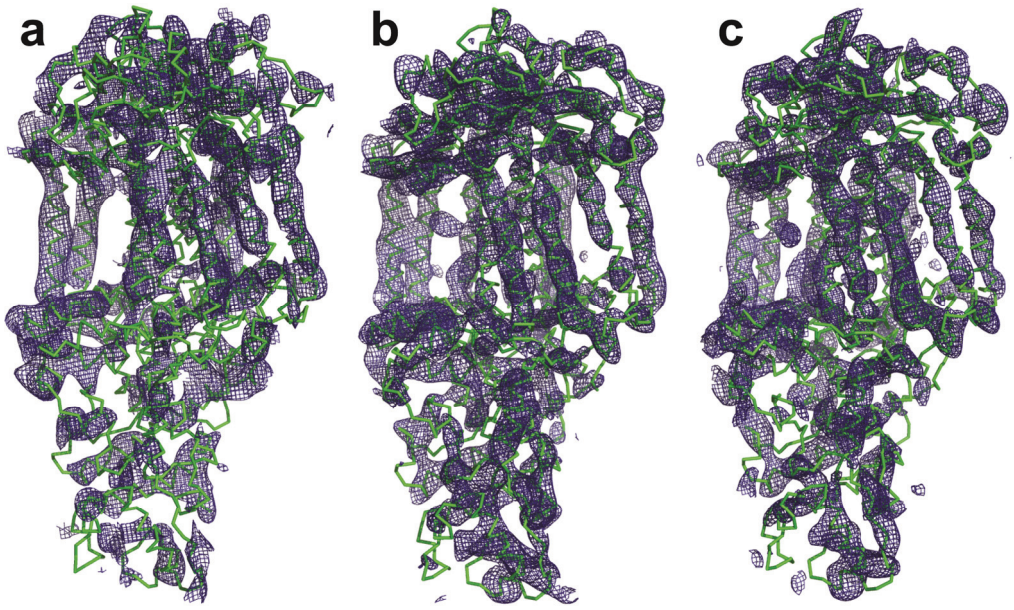

Composite omit electron density maps calculated using CNS 1.3 with 5 % of the model removed in each step: (**a**) Calculated using LCLS data; (**b**) Calculated from data extracted from PDB entry 2wjn; (**c**) Calculated from data extracted from PDB entry 2x5u. All data are cut to 8.2 Å resolution and all maps are contoured at 1.5 σ.

Supplementary Figure 6: Electron density maps with hemes omitted.

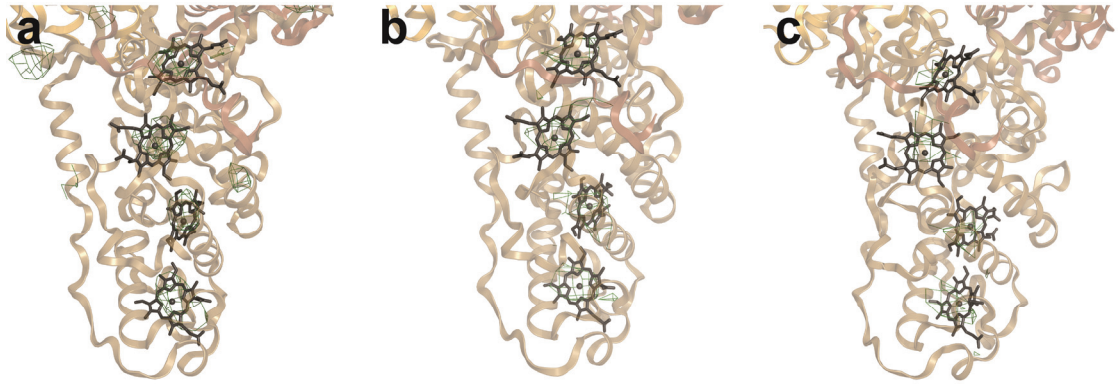

Omit electron density maps calculated with the heme co-factors of the cytochrome subunit removed: (**a**) Calculated using LCLS data; (**b**) Calculated from data extracted from PDB entry 2wjn; (**c**) Calculated from data extracted from PDB entry 2x5u. All data are cut to 8.2 Å resolution and all maps are contoured at 2 σ.

Supplementary Figure 7: PEG-based LSP microjet images.

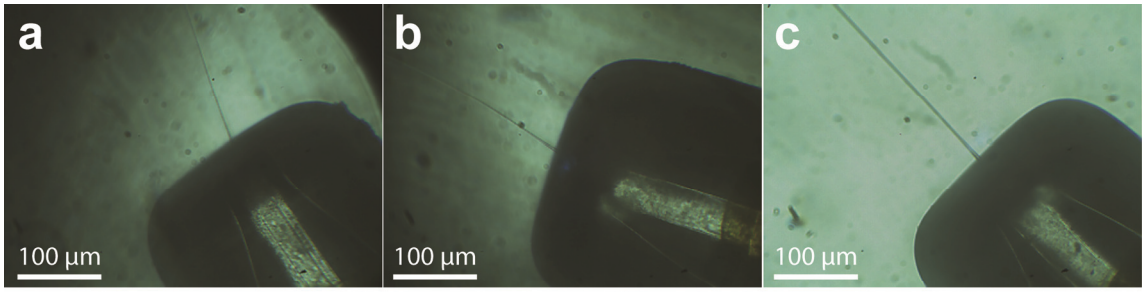

Microjets formed using PEG-based LSP: (**a**) PEG400 (40 %), Monoolein (30 %) and buffer (30 %); (**b**) PEG1500 (40 %), Monoolein (30 %) and buffer (30 %); (**c**) PEG4000 (40 %), Monoolein (30 %) and buffer (30 %).

Supplementary Figure 8: Diffraction image from a mosaic crystal.

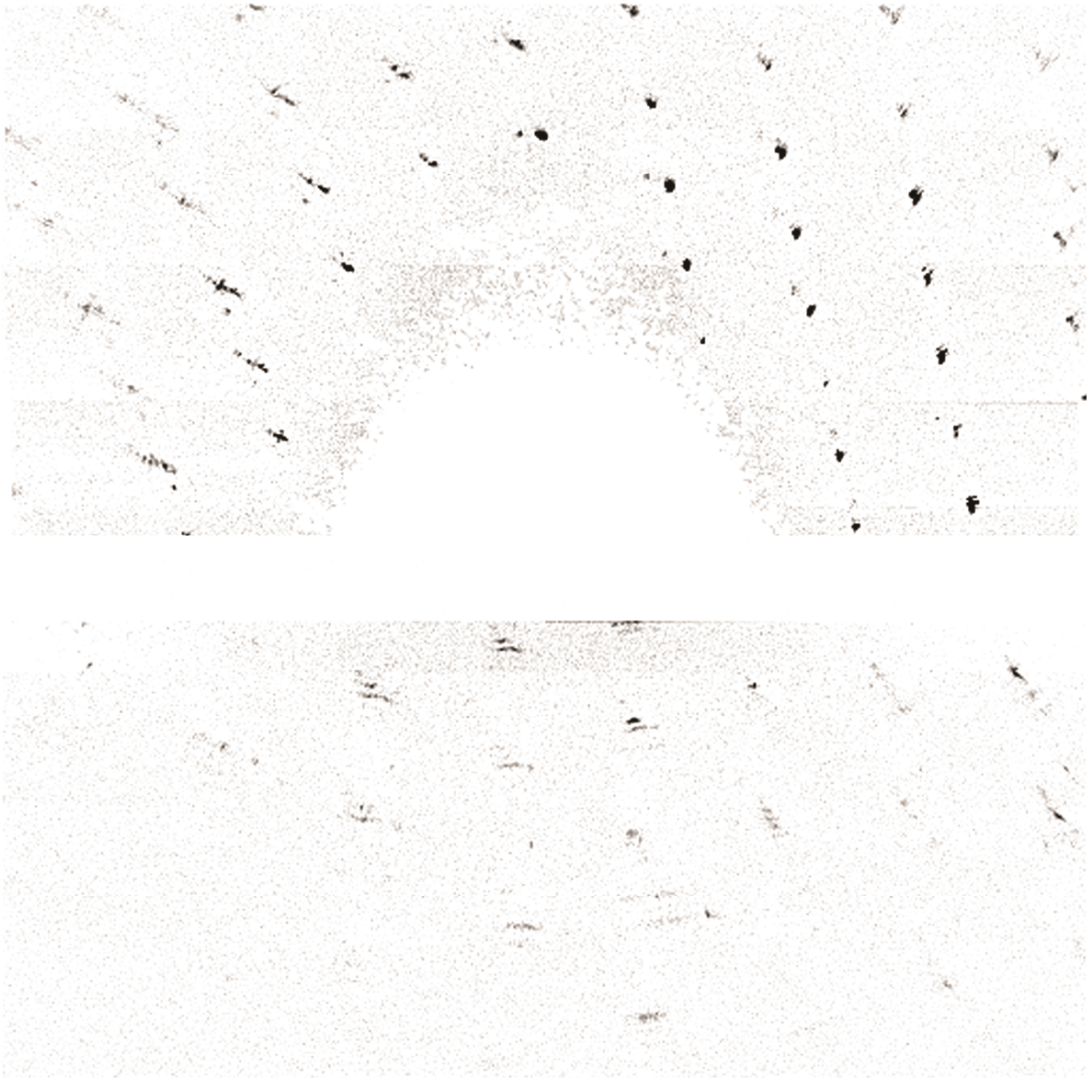

Example of a microcrystal diffraction image that could not be processed due to its high mosaic spread.

Supplementary Figure 9: NZ-test and L-test plots.

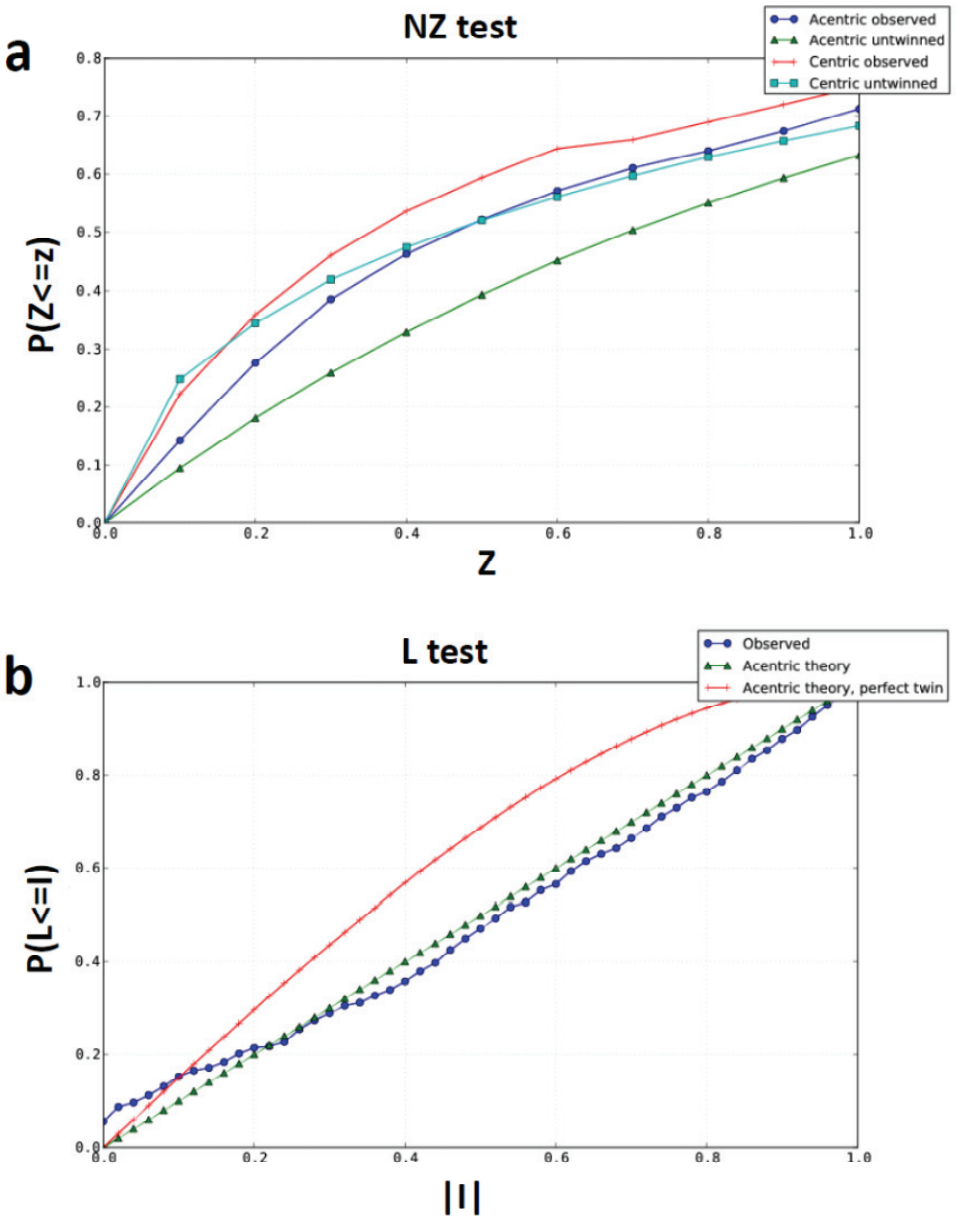

(**a**) NZ-plots and (**b**) L-test for the serial femtosecond crystallography data, calculated with the xtriage program of the Phenix[18] package.

Supplementary Figure 10: Electron density maps against control data.

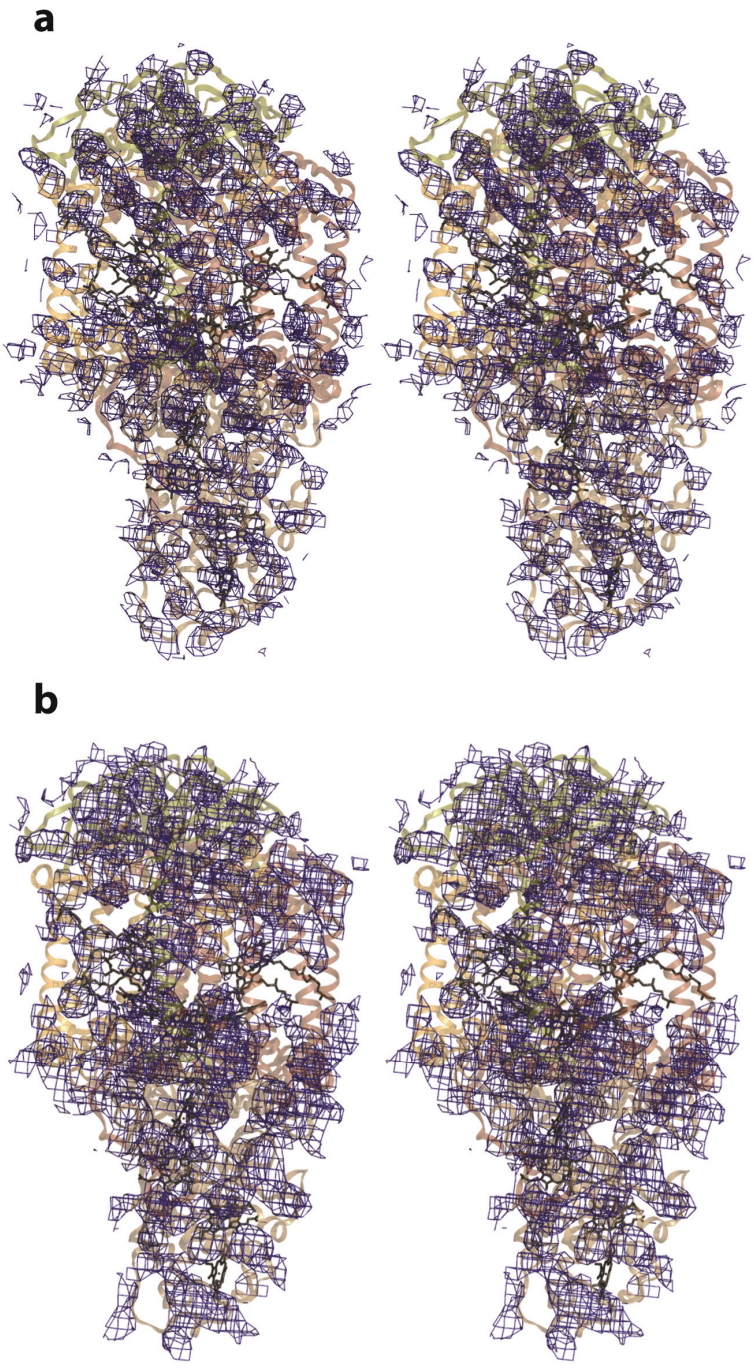

Control $2mF_{obs}$-DF_{calc} electron density maps calculated using the molecular replacement solution in **Supplementary Figure 4** against control data where: (**a**) h,k,l indicies of processed data are randomly shuffled; and (**b**) Intensities are set to be uniform. Both maps are contoured at 1σ.

Supplementary Table 1: Summary of deposited structures solved using Lipidic cubic phase (LCP) and lipidic sponge phase (LSP)

Protein	Resolution (Å)	Source	PDB entry	Method	Year	lipidic phase structure
Bacteriorhodopsin	2.50	*H. salinarum*	1AP9	LCP	1997	Pebay-Peyroula et al.
Halorhodopsin	1.80	*H. salinarum*	1E12	LCP	2000	Kolbe et al.
Sensory rhodopsin II	2.10	*N. pharaonis*	1H68	LCP	2001	Royant et al.
Sensory rhodopsin II-transducer complex	1.94	*N. pharaonis*	1H2S	LCP	2002	Gordeliy et al.
Reaction center	2.35	*R. sphaeroides*	1OGV	LCP	2003	Katona et al.
Anabaena Sensory Rhodopsin	2.00	*Anabaena*	1XIO	LCP	2004	Vogeley et al.
Engineered human β_2 adrenergic receptor	2.40[§]	*Homo sapiens*	2RH1	LCP*	2007	Cherezov et al.
OpcA outer membrane adhesion	1.95	*N. meningitidis*	2VDF	LCP*	2007	Cherezov et al.
Human A_{2A} adenosine receptor	2.60	*Homo sapiens*	3EML	LCP*	2008	Jaakola et al.
Reaction center	2.20	*R. sphaeroides*	2GNU	LSP	2006	Wadsten et al.
Light harvesting complex II	2.45	*Rps. Acidophila*	2FKW	LSP	2006	Cherezov et al.
BtuB	1.95	*E. coli*	2GUF	LSP	2006	Cherezov et al.
Reaction center	1.86	*Bl. viridis*	2WJN	LSP	2009	Wöhri et al.
CXCR4 Chemokine receptor	2.50[§]	*Homo sapiens*	3ODU	LCP*	2010	Wu et al.
Dopamin D3 receptor	3.15	*Homo sapiens*	3PBL	LCP*	2010	Chien et al.
ba_3 cytochrome c oxidase	1.80	*T. thermophilus*	3S8F	LCP*	2011	Tiefenbrunn et al.
Histamine H1 receptor	3.10	*Homo sapiens*	3RZE	LCP*	2011	Shimamura et al.

* Originally reported as LCP crystallization but likely to have proceeded *via* LSP since PEG400 was added in excess.
§ Highest resolution reported

Supplementary Table 2: X-ray data and refinement statistics

Total number of images	365,035
Images showing diffraction	1542
Images indexed	265
Wavelength	6.17 Å
Data processing resolution limits	46.1 - 7.4 Å
Number of used reflections	2247
Completeness	85 %
Multiplicity	8.0
$^{\dagger}R_{int}$	50%
I/σ	1.9
Refinement resolution limits	46.1 - 8.2 Å
R_{factor}	35 %
R_{free} (5% omitted reflections)	38 %
Overall figure of merit	0.62

$^{\dagger}R_{int} = \Sigma_{hkl} |F_{even}-F_{odd}|/\Sigma_{hkl} ((F_{even}+F_{odd})/2)$ as defined in[16].
R_{int} is not equivalent to R_{merge} (familiar from standard crystallography) due to the challenges associated with processing partial Bragg reflections in serial femtosecond crystallography.
Resolution shell breakdowns in Supplementary Tables 1 and 2.

Supplementary Table 3: Crystallographic data statistics by resolution shell.

d_{max} (Å)	No. of unique reflections	Completeness (%)	$R_{int}(F)$	<I/sigma>	Multiplicity
15.88	311	96.3	53.0	1.9	12.0
12.60	294	100.0	46.5	1.9	12.6
11.01	280	100.0	45.8	1.9	13.3
10.00	279	99.6	42.7	1.7	9.6
9.29	261	99.6	55.4	1.8	7.1
8.74	276	97.2	63.2	1.7	5.3
8.30	255	95.5	54.3	2.2	4.2
7.94	243	90.3	45.9	2.0	3.4
7.63	176	64.7	71.8	1.8	1.9
7.37	56	21.5	n/a	n/a	1.1
7.37	2431	87.1	49.7	1.9	8.0

Supplementary Table 4: Refinement statistics by resolution shell.

d_{max} (Å)	R_{work}	R_{free}
22.4	0.46	0.35
18.3	0.47	0.35
15.8	0.39	0.42
14.1	0.32	0.34
12.9	0.38	0.37
12.0	0.29	0.41
11.2	0.31	0.31
10.5	0.31	0.53
10.0	0.34	0.34
9.5	0.27	0.25
9.1	0.38	0.35
8.8	0.34	0.33
8.5	0.34	0.37
8.2	0.38	0.80
8.2	0.35	0.38

SUPPLEMENTARY NOTE

Lipidic cubic and sponge phase crystal structures. Lipidic cubic phase crystallization initially led to rapid advances with the structural biology of archaeal rhodopsins[1-5] and more recently concerning the structural biology of G-protein coupled receptors[6-10] (**Supplementary Table 1**). The closely related approach of lipidic sponge phase crystallization has produced four independent membrane protein structures to date[11-14]. It also appears likely that the crystals used for structural determination of several G-protein coupled receptors[6-10] and one bacterial oxidase[15] also grew *via* a cubic-to-sponge-phase transition (**Table 1**) since all were grown in excess PEG400.

I/σ estimates. Data were processed using a Monte-Carlo integration method[16,17]. In this approach σ_{hkl} is defined as the root-mean-square deviation of spot intensity values from their mutual mean, $\langle I_{hkl} \rangle$, divided by the square root of the number of spots (N):

$$\sigma_{hkl} = \frac{\sqrt{\sum_{N} \left(I_{spot} - I_{hkl} \right)^2}}{N}$$

Significant variations emerge because all observations are partial reflections, crystal orientations are sampled randomly, there are variations in crystal shapes and sizes, and there are fluctuations in the X-FEL beam spatial and energy profile. I/σ ratios improve with N (approximately as $\sqrt{N}$) because improved multiplicity causes σ to decrease. Chapman *et al.*[17] reported a multiplicity of 706 for all data collected from microcrystals of PSI and an overall I/σ of 12.2 was recovered. In this work a multiplicity of 8 was observed for all data and this resulted in an overall I/σ of 1.9 that showed little variation with resolution shells.

Supplementary References.

1. Pebay-Peyroula, E., Rummel, G., Rosenbusch, J.P. & Landau, E.M.*Science* **277**, 1676-81 (1997).
2. Kolbe, M., Besir, H., Essen, L.O. & Oesterhelt, D. *Science* **288**, 1390-6 (2000).
3. Royant, A. et al. *Proc. Natl. Acad. Sci. USA* **98**, 10131-6 (2001).
4. Gordeliy, V.I. et al. *Nature* **419**, 484-7 (2002).
5. Vogeley, L. et al. *Science* **306**, 1390-3 (2004).
6. Cherezov, V. et al. *Science* **318**, 1258-65 (2007).
7. Jaakola, V.P. et al. *Science* **322**, 1211-7 (2008).
8. Wu, B. et al. *Science* **330**, 1066-71 (2010).
9. Chien, E.Y. et al. *Science* **330**, 1091-5 (2010).
10. Shimamura, T. et al. *Nature* **475**, 65-70 (2011).
11. Wadsten, P. et al. *J. Mol. Biol.* **364**, 44-53 (2006).
12. Cherezov, V., Clogston, J., Papiz, M.Z. & Caffrey, M. *J. Mol. Biol.* **357**, 1605-18 (2006).
13. Cherezov, V. et al. *J. Mol. Biol.* **364**, 716-34 (2006).
14. Wohri, A.B. et al. *Biochemistry* **48**, 9831-8 (2009).
15. Tiefenbrunn, T. et al. *PLoS One* **6**, e22348 (2011).
16. Kirian, R.A. et al. *Acta Crystallogr. A* **67**, 131-40 (2011).
17. Chapman, H.N. et al. *Nature* **470**, 73-7 (2011).
18. Adams, P.D. et al. *Acta Crystallogr D Biol Crystallogr* **66**, 213-21 (2010).